NUKLEONIKA 2004;49(1):15–21

ORIGINAL PAPER

The influence of defect structure on the surface sputtering of metals under irradiation of swift heavy ion in the inelastic energy loss region

Yurii N. Cheblukov,
Alexander Yu. Didyk,
Andrzej Hofman,
Vera K. Semina,
Wojciech Starosta

Abstract The results of the influence of heavy ion irradiation in the inelastic energy loss region on the structure of some metals such as nickel, single crystal tungsten, chromium-nickel stainless steel and cold-deformed gold are presented. It was shown that the sputtering (evaporation) yield strongly depends on the density of defects in these metals. The sputtering yield starts to grow strongly with the increase of damages created by elastic and inelastic energy heavy ion losses. The stainless steel surface structure behaved differently under irradiation than the pure metal surface structure.

Key words defect concentration effect • ion irradiation • ion track temperature • metals • sputtering • surface structure

Yu. N. Cheblukov
Institute of Theoretical and Experimental Physics,
25 Bolshaja Cheremushkinskaya Str.,
117259 Moscow, Russia

A. Yu. Didyk✉, V. K. Semina
Joint Institute for Nuclear Research, FLNR,
141980 Dubna, Russia,
Tel.: 7 09621 63376, Fax: 7 09621 65955,
e-mail: didyk@main1.jinr.ru, didyk@cv.jinr.ru,
didyk52@mail.ru

A. Hofman
Joint Institute for Nuclear Research, FLNR,
141980 Dubna, Russia
and Institute of Atomic Energy,
04-400 Otwock-Świerk, Poland

W. Starosta
Institute of Nuclear Chemistry and Technology,
16 Dorodna Str., 03-195 Warsaw, Poland

Received: 18 July 2003, Accepted: 30 December 2003

Introduction

Research on the influence of irradiation with swift heavy ions in the inelastic energy loss region began to develop intensively in the last 15–20 years in many accelerator centers. As it is well known, the problems of ion track creation were connected with two old models: the Coulomb explosion model and the thermal spike (thermal peak) one. With the development of some new methods for studying irradiated surfaces, such as scanning tunneling (STM) and atomic force microscopy (AFM), the investigation possibilities of irradiated surfaces gained a new life.

It is very interesting to study the interaction of swift heavy ions with metals, dielectrics, semiconductors and amorphous alloys. Some investigations showed that the structure of the volume around the heavy ion trajectory consists of a core with radius $R_1 \sim 50$ Å, which has a high damage density, and a less-damaged volume around this core with the radius larger than the core radius ($R_2 \sim 100$ Å) [11].

Research on the sputtering of coarse-grained metals by swift heavy ions was started about ten years ago in connection with acceleration and storage requirements for high-intensity heavy ion drivers [2]. The sputtering yields of annealed coarse-grained gold with high-energy ^{238}U and ^{84}Kr ions have been measured experimentally [6, 13], and experimental data on the sputtering of Au, Zr and Ti by Au swift ions were obtained recently [1]. As shown by an analysis of experimental data [1, 6, 13], the difference between the experimentally measured and the calculated sputtering yield according to the cascade theory is generally negligible.

Heavy ions will irradiate in the so-called driver metals, where they create defects in the initial polycrystalline structure due to elastic collisions. These defects persist during irradiation. In this case sputtering mechanism can change [3, 15].

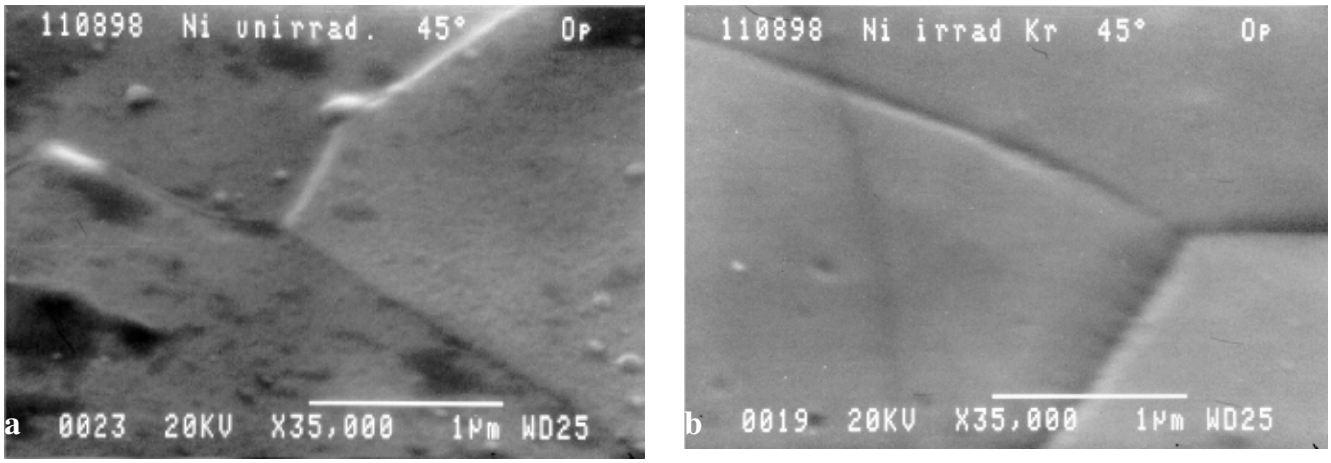

Fig. 1. The surface structure of polycrystalline Ni before (a) and after irradiation (b) with 305 MeV ^{86}Kr ions up to the fluence $F{\cdot}t = 2 \times 10^{15}$ ions/cm^2.

The purpose of this article is to verify the applicability of the thermal spike model for the description of sputtering processes and track creation in metals and alloys at high fluences. We investigated surface structure changes during ion irradiation of some metals and alloys.

Experimental method and results of metal sputtering under irradiation with swift heavy ions at high fluences

Samples of the studied metals and alloys such as polycrystalline Ni, single-crystal W and chromium-nickel stainless steel (SS) were annealed at 700°C for 1 h in a vacuum of 10^{-3} Pa, then were electrochemically polished and were irradiated in a set-up described recently [16, 17]. The irradiation was carried out with ^{86}Kr ions up to the fluences 10^{15} ions/cm^2 or more [4, 5, 9, 10]. Before and after irradiation the samples were characterized by means of a scanning electron microscope (JSM-840).

The scanning electron microscopy (SEM) images for Ni are presented in Fig. 1, where Fig. 1a is the initial surface and Fig. 1b shows the surface after irradiation with 305 MeV ^{86}Kr ions up to the fluence $F{\cdot}t = 2 \times 10^{15}$ ions/cm^2. One can see that the metal surfaces were polished by irradiation, and surface irregularities are sputtered. Furthermore, it is possible to see a considerable material sputtering near the grain boundaries. The yield of the grain boundary sputtering S_{ex} is found to be larger than 2000 atoms/ion. This sputtering yield has been obtained by an estimate of the volume of the material sputtered on grain boundary.

Then, to estimate the sputtering yield for a crystallite, the previously irradiated nickel sample was re-irradiated using a mask. The mask was placed over a half of the irradiated surface and then the exposed area was irradiated with 245 MeV ^{86}Kr ions up to the fluence of $F{\cdot}t = 1 \times 10^{15}$ ions/cm^2. The thickness of the sputtered Ni layer, was estimated by the difference between the thickness for single- and double-irradiated parts of the sample being the height of the step (see Fig. 2), which was $h \approx 0.35$ μm, and which allowed to obtain a sputtering yield at $S_{Ni} = 3000$ atoms/ion.

Double irradiation allows the decrease of possible swelling influence on the experimental measured value of sputtering yield. The nickel swelling can only decrease the estimations of the sputtering yield in this experiment. Higher yields of grain boundary sputtering may be explained by its initial structure, because the area near grain boundary initially has a very developed defect structure with high defect concentration.

The STM-images of the surface structures for nickel grain body are presented in Fig. 3. One can see the initially electrochemically polished nickel surface structure before (Fig. 3a) and after irradiation (Fig. 3b) with 305 MeV ^{86}Kr ions up to the fluence $F{\cdot}t = 2 \times 10^{15}$ ions/cm^2. The images (scans) were obtained by the STM technique. The difference between the relief heights for unirradiated (Fig. 3a) and irradiated (Fig. 3b) samples, is very high: ≈54 nm and ≈12 nm, respectively. The average height values have been calculated using a number of scans for unirradiated and irradiated nickel samples. These values turned out to be $H_a \approx 47$ nm and $H_b \approx 21$ nm. The approximate value of the number of atoms, N_{NiS}, evaporated (sputtered) from the nickel surface under the irradiation with ^{86}Kr ions have been estimated by a simple expression

$$(1) \qquad N_{NiS} \sim (H_a - H_b) \cdot N_{Ni} = 2.4 \times 10^{17} \text{ atoms/cm}^2$$

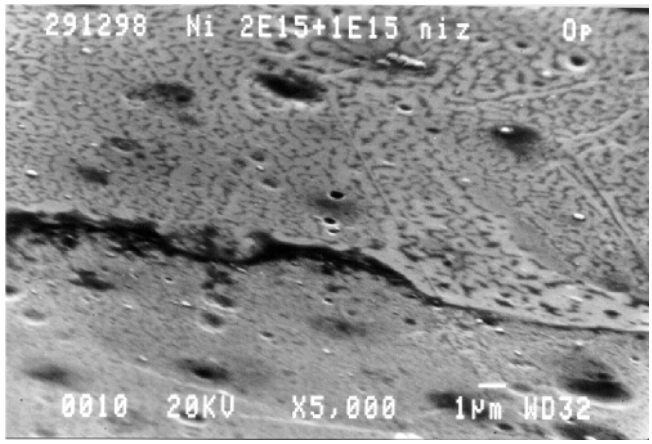

Fig. 2. The surface structure of polycrystalline Ni previously irradiated with 305 MeV ^{86}Kr ions up to the fluence $F{\cdot}t = 2 \times 10^{15}$ ions/cm^2 and then irradiated with 245 MeV ^{86}Kr ions up to the fluence of $F{\cdot}t = 1 \times 10^{15}$ ions/cm^2 (the upper part was covered by mask). One can see a step on the boundary between single- and double-irradiated regions.

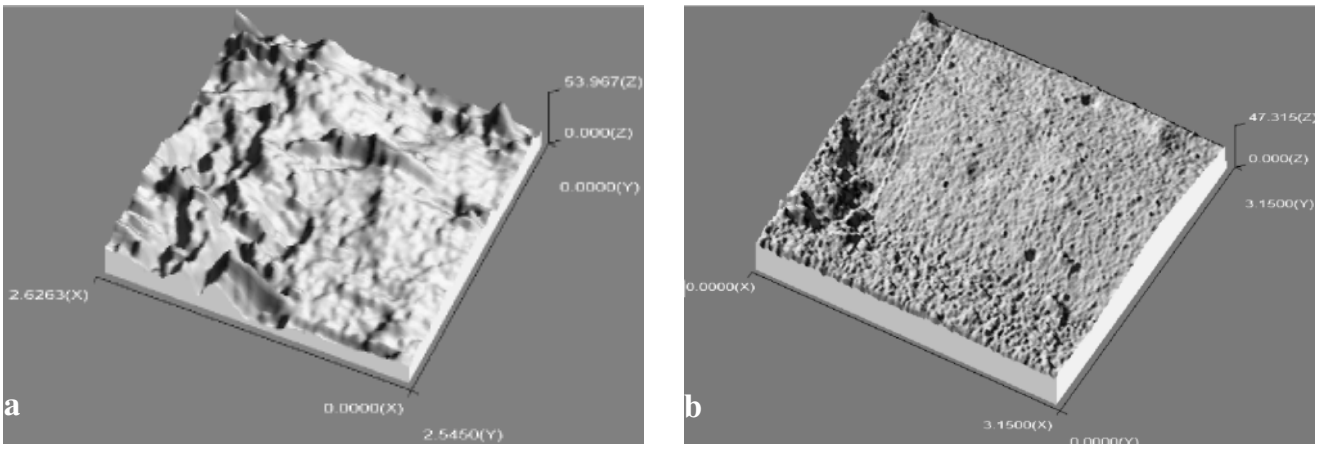

Fig. 3. The surface structures of polycrystalline nickel in initial state (a), the scanning area is 2.6 μm × 2.5 μm and height is 54 nm, and after irradiation with 305 MeV Kr ions up to the fluence $F{\cdot}t = 2 \times 10^{15}$ ions/cm^2 (b), the scanning area is 3.15 μm × 3.15 μm and height is 47 nm. The images were obtained by means of STM technique.

where: $N_{Ni} = 9.1 \times 10^{22}$ atoms/cm^3 is the number of nickel atoms per 1 cm^3. So the sputtering coefficient (or, most probably, the evaporation coefficient) is $S_{ex} > N_{NiS}/(F{\cdot}t) = 1.2 \times 10^2$ atoms/ion.

The presence of radiation defects in metals has an influence on the sputtering yield. Thus, the sputtering yield for metal having a low defect concentration in the crystalline structure is in the range of 1–10 atoms/ion [1, 6, 15]. An experiment [9] has shown that the sputtering yield for coarse-grained metals irradiated with swift heavy ions increases by a factor of 10^2–10^3 at high irradiation fluences ($F{\cdot}t = 2 \times 10^{15}$ ions/cm^2) at the expense of accumulating radiation defects in the target crystalline structure. The high sputtering yield for nickel observed experimentally is possibly explained by atom evaporation from the ion track surface, which has been heated up to the temperature higher than the boiling point. The observed effects can be understood on the basis of the following model.

The time for energy transfer from electrons heated with heavy ions to lattice atoms is $t \approx 10^{-12}$ s, and lattice atoms cannot obtain high temperature [7, 8, 14, 18]. In the case of the crystal with high defect concentration, the energy transfer time can decrease down to 10^{-13} s and the temperature of lattice around the ion trajectory must be very high. It can cause the lattice melting and ion track creation. The final temperature on the track axis θ(0) may be estimated with the help of the following expression [18]

$$\theta(0) = \sqrt{\frac{8\pi}{9} \cdot \frac{\hbar S^2}{a} N \sigma_0 r_0^2 \cdot \frac{\alpha}{b} T_0^{1/2} \left[\left(\frac{T_0}{\varepsilon_F} \right)^{3/2} - 1 \right]} \quad (2)$$

where: $\sigma_0 = 2\pi a_0^2$, a_0 is the Bohr radius; S is the acoustic velocity; N is the atom density for target material; r_0 is the initial radius of excited electrons area ($r_0 \sim 1$ nm); T_0 is the initial electron temperature in the excited area; a is the lattice constant; α and β are the constants (for Fe $\alpha = 0.05$ eV^{-1} and $\beta = 0.1$ eV^{-1}); ε_F is the Fermi energy; b is a material constant. The initial electron temperature in the excited area T_0 and the b value can be calculated as

$$T_0 = \sqrt{\frac{(\partial E / \partial x)_{inel}}{\pi r_0^2 N (1.5\alpha + \beta)}}, \quad b = \frac{\alpha\gamma}{3\alpha + 2\beta} \quad (3)$$

where: $\gamma = 0.033$ cm^2 s^{-1}eV$^{-3/2}$ for Fe [18]. For example, for the U ions in Fe $T_0 \cong 40$ eV; for gold and iron $b_{Au} = 0.0124$ cm^2 s^{-1}eV$^{-3/2}$ and $b_{Fe} = 0.0047$ cm^2 s^{-1}eV$^{-3/2}$.

Using equation (2), it is possible to estimate the temperature in ion track area (for the U ions with $(\partial E/\partial x)_{inel}$ ~100 keV/nm the $\theta(0) \approx 0.4$ eV, i.e. $T_{tr} \equiv \theta(0)/k_B \cong 4600$ K, where k_B – Boltzmann's constant). Practically, the same order of temperature values ($T_{tr} > T_{melt}$) follows from the expression for temperature calculations presented in [7, 8, 14].

Thus, the processes of Ni atom evaporation must take place with the growth of damage concentration. The given expressions for temperature calculation are accurate only at high damage concentration in metals. And this fact allows one to understand such a high sputtering yield for Ni.

Studies of sputtering yields for W single crystal, stainless steel Cr18Ni10 (SS) and cold-deformed gold were carried out for a comparison.

The surface of chromium-nickel stainless steel (Cr18Ni10T) in the initial state before irradiation is shown in the Fig. 4a. Figure 4b shows the SS surface structure after irradiation with ^{86}Kr ions with a fluence up to $F{\cdot}t = 2.6 \times 10^{15}$ ions/cm^2. As one can see, the irradiated surface exhibits an interesting structure. The irradiated surface is covered by the so-called hillocks. The ion irradiation fluence was the same as in the case of Ni. Analogous surface structure of SS irradiated with 124 MeV ^{129}Xe ions was recently observed by the authors at very high fluences [8]. The strange hillock structure on the irradiated stainless steel surface should be studied in future experiments.

The initially electrically polished surface of a tungsten single crystal before irradiation is shown in Fig. 5a and the same surface after irradiation with 305 MeV ^{86}Kr ions up to the fluence $F{\cdot}t = 2 \times 10^{15}$ ions/cm^2 is shown in Fig. 5b. The images were obtained by scanning electronic microscopy (SEM). The initial tungsten single crystal showed a ratio of its resistivity at room temperature to that at liquid helium temperatures of $\rho(300\text{ K})/\rho(4.2\text{ K}) \cong 80{,}000$.

To estimate the surface relief inhomogeneities on small areas, the scanning tunneling microscopy (STM) was used. The surface structures of the initial tungsten crystal (Fig. 6a) and the one irradiated with 305 MeV ^{86}Kr ions up to the fluence $F{\cdot}t = 2 \times 10^{15}$ ions/cm^2 (Fig. 6b) are presented. As one can see from these figures, the difference between the

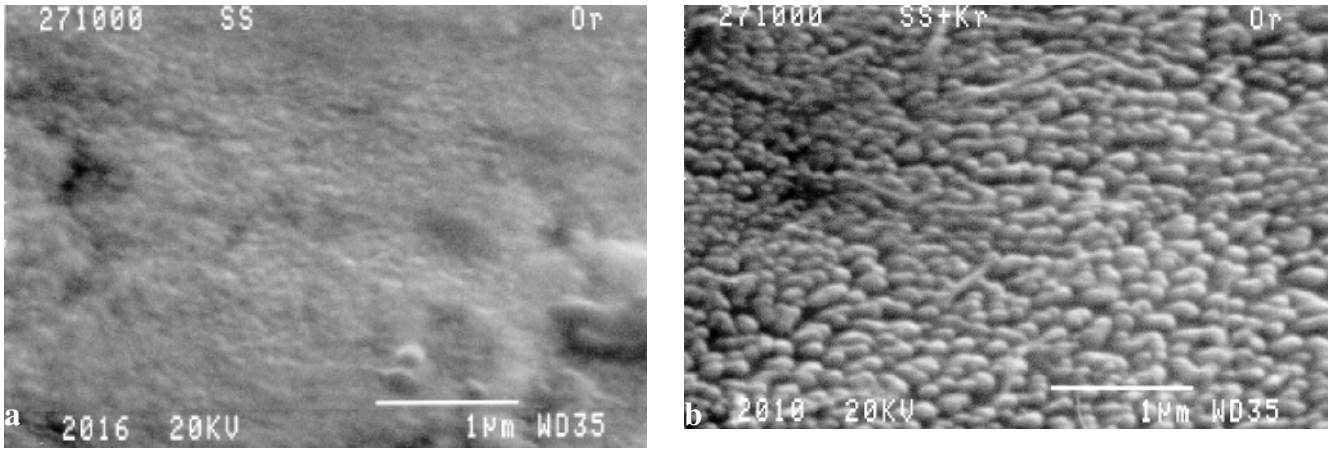

Fig. 4. The stainless steel surface structure in initial state (a) and after irradiation (b) with 245 MeV ^{86}Kr ions up to the fluence $F{\cdot}t = 2.6 \times 10^{15}$ ions/cm^2. The images were obtained by means of SEM technique.

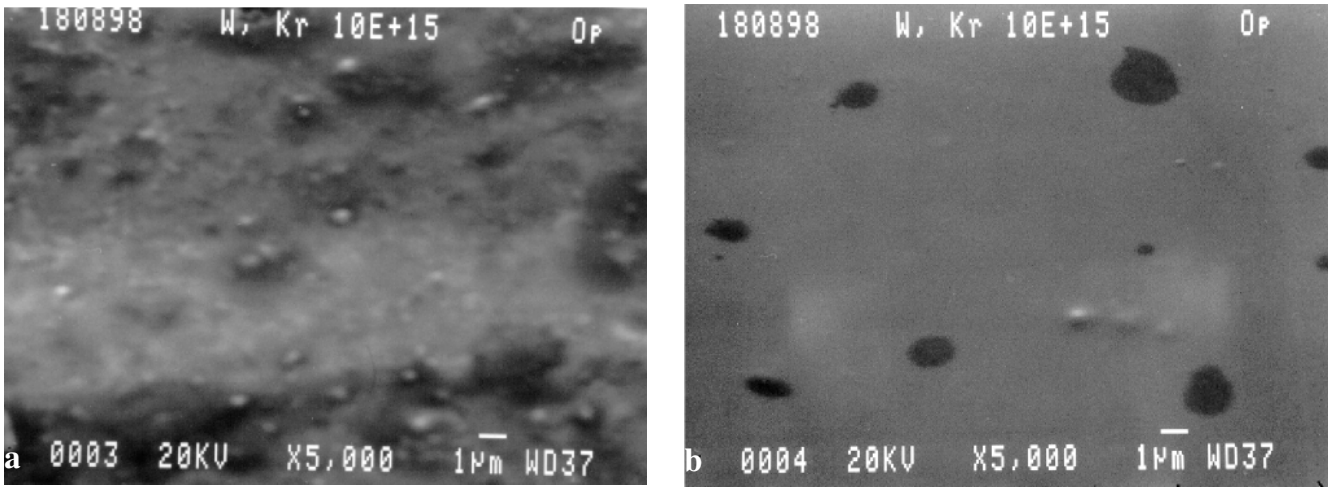

Fig. 5. The tungsten surface structures in initial state (a) and after irradiation (b) with 305 MeV ^{86}Kr ions up to the fluence $F{\cdot}t = 2 \times 10^{15}$ ions/cm^2. The images were obtained by means of SEM technique.

heights of unirradiated and irradiated sample parts is significant: 76 nm and ≈9 nm, respectively. We have calculated the average height values using a lot of scans for unirradiated and irradiated tungsten. These values turned out to be $H_a = 61$ nm and $H_b = 22$ nm.

The approximate value of numbers of atoms evaporated (sputtered) from the tungsten metal surface under irradiation with ^{86}Kr ions, N_{WS}, has been estimated by means of expression (1). So, one obtains $N_{WS} \sim (H_a - H_b) \cdot N_W = 2.5 \times 10^{17}$ atoms/cm^2, where $N_W = 6.3 \times 10^{22}$ atoms/cm^3 is the

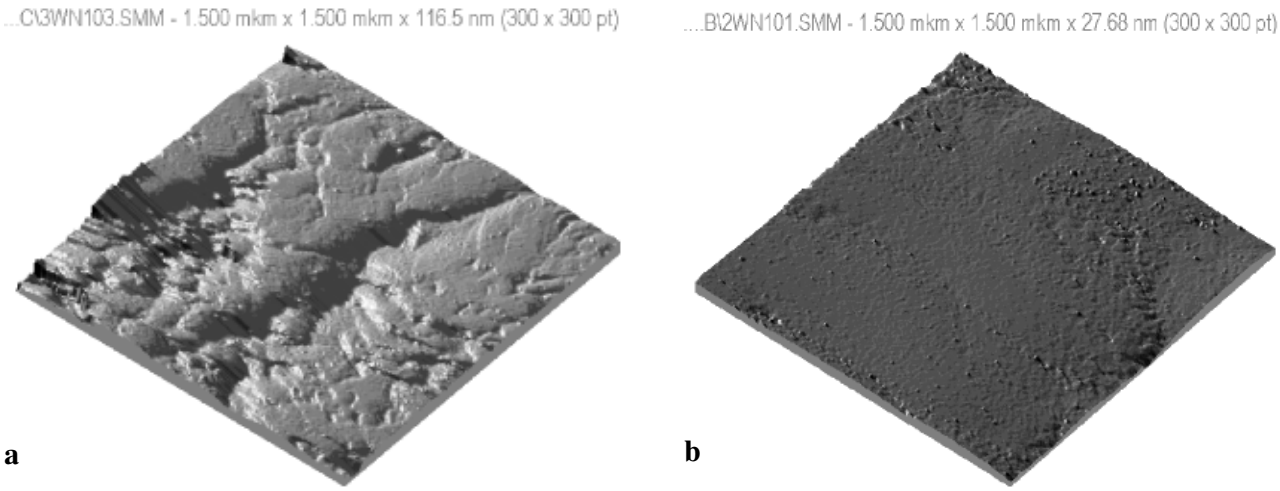

Fig. 6. The tungsten surface structures in initial state (a) and after irradiation (b) with 305 MeV Kr ions up to the fluence $F{\cdot}t = 2 \times 10^{15}$ ions/cm^2. The scanning area is 1.5 μm × 1.5 μm, the relief heights are 116.5 nm (a) and 27.7 nm (b). The images were obtained by means of STM technique.

Table 1. SRIM-calculated values of projected range R_p, inelastic energy loss $S_{inel} = (dE/dx)_{inel}$, track temperature T_{tr}, sputtering yield S_y, crater diameter D_{evap} for irradiation with 245 MeV ^{86}Kr irradiation and published data about melting point T_{melt} for nickel, stainless steel (SS) and tungsten.

Material	Ni	SS	W
R_p (μm)	14.2	15.4	11.9
S_{inel} (MeV/μm)	28	24.5	35
T_{tr} (K)	1.04 ± 10^4	0.95 ± 10^4	2 ± 10^4
T_{melt} (K)	1728	1673	3693
S_y (atoms/ion)	>120	>100	>126
Crater diameter, D_{evap} (Å)	>17	>16	>20

number of tungsten atoms per 1 cm^3. In such a manner the sputtering coefficient (or, most probably, the evaporation coefficient) is roughly $S_{ex} \cong N_{WS}/(F{\cdot}t) = 1.2 \times 10^2$ atoms/ion.

Calculated values of projected ranges R_p and inelastic energy losses $S_{inel} = (dE/dx)_{inel}$ for the Ni, W and SS targets are presented in Table 1. To estimate the temperature on the track axis using theoretical S_{inel} values, we used the following simple expression [7, 11]

$$T_{tr} = \frac{S_{inel}(x)}{\pi R_{tr}^2 C_i \rho_i} + T_0. \quad (4)$$

Here C_i – heat specific capacity; ρ_i – material density; R_{tr} – track radius; T_0 – irradiation temperature. The S_{inel} calculations were performed by means of a computer code SRIM.

The pressure in the area around the hot ion track at the temperature $T_{tr} \sim 10^4$ K (without volume changes) is approximately 10^2 kbar [12]. So, the target atoms can be thrown out from the surface by high pressure, too.

We will use a simple model for evaporation: the target atoms can be evaporated from a cone with the diameter D_{evap} and the depth H_{evap}, and $H_{evap} \approx D_{evap}$. Then the number of atoms "sputtered" by one ion S_{ex} can be expressed as

$$S_{ex} = N_{mat} \cdot V_1 = N_{mat} \cdot \frac{\pi D_{evap}^2}{12} \quad (5)$$

where N_{mat} is the number of atoms in 1 cm^3 and V_1 is the volume of one crater. The total evaporated metal volume, V_{tot}, from surface with area 1 cm^2 was estimated from SEM-images, and the sputtering-evaporation coefficients were calculated by the expression

$$S_{ex} = \frac{N_{mat} \cdot V_{tot}}{F \cdot t}. \quad (6)$$

Then the volume of one crater, V_1, is equal to $V_1 = V_{tot}/F{\cdot}t$ and the diameters D_{evap} were calculated using expression (5).

The sputtering coefficients for annealed gold foils irradiated with ^{238}U, ^{196}Au and ^{86}Kr swift heavy ions are presented in Table 2 [1, 6, 15]. As one can see, the experimental values of sputtering coefficient are $S_{ex} \approx 1$–12 atoms/ion. The Au sputtering coefficients calculated with the help of the cascade sputtering model (S_{CT}) differ from experimental values substantially, especially for irradiation with ^{238}U and ^{196}Au ions with a high level of inelastic energy losses. The calculated projected ranges of ^{238}U, ^{196}Au and ^{86}Kr ions in Au, the elastic cross-section near the surface σ_d and inelastic energy losses $(dE/dx)_{inel}$ are presented in Table 3. In the calculations of displacement cross-section under elastic ion collisions with Au atom, σ_d, the threshold energy was taken as $E_d = 20$ eV.

As one can see, the elastic cross-section of the Au atom displacement, σ_d, has the highest value when the annealed gold thick foil is irradiated with ^{196}Au ion, but the sputtering coefficient S_{ex} is less in comparison with irradiation with ^{238}U ions: 9 and 12 atoms/ion, respectively. This difference between the sputtering coefficients cannot be explained by using only elastic collisions. It is necessary to take into account also the inelastic energy loss and the temperature effects (thermal spike model). The inelastic energy loss $(dE/dx)_{inel}$ for ^{238}U is larger than for ^{196}Au ion irradiation by a factor of ~1.8.

Then the gold samples (gold purity 99.9%) underwent cold deformation to create high concentration of dislocations and were irradiated with 253 MeV ^{84}Kr ions up to the fluence $(F{\cdot}t) = 10^{14}$ ions/cm^2. The initial gold surface was very smooth. The mean ion flux was $F = 3.7 \times 10^9$ ions/(cm^{2}s) during irradiation. The images of initial (Fig. 7a, Fig. 7c) and irradiated with ^{86}Kr ions (Fig. 7b,

Table 2. The experimental sputtering yield in the inelastic energy loss range for the polycrystalline gold targets irradiated with ^{238}U, ^{196}Au and ^{86}Kr heavy ions.

Ion/Target	Energy (MeV)	Sputtering yield, experiment, S_{ex} (atoms/ion)	Sputtering yield, cascade theory, S_{CT} (atoms/ion)	Inelastic energy loss, $(dE/dx)_{inel}$ (keV/Å)
^{238}U/^{196}Au	1400	12 ± 2	≤ 1	9.82
^{196}Au/^{196}Au	230	9.3 ± 0.9	~ 3	5.52
^{86}Kr/^{196}Au	200	1.0 ± 0.2	≤ 1	3.28

Table 3. The calculated values of projected ranges (R_p), elastic cross-section near the surface σ_d, and inelastic energy losses $(dE/dx)_{inel}$ for the ^{238}U, ^{196}Au and ^{86}Kr heavy ions in Au.

Ion/Target	Energy (MeV)	Projected range, R_p (μm)	Inelastic energy loss, $(dE/dx)_{inel}$ (keV/Å)	Elastic cross-section, σ_d (dpa·cm^2/ion)
^{238}U/^{196}Au	1400	21.26	9.82	3.7×10^{-16}
^{196}Au/^{196}Au	230	7.65	5.5	1.1×10^{-15}
^{86}Kr/^{196}Au	253	10.78	3.33	1.65×10^{-16}

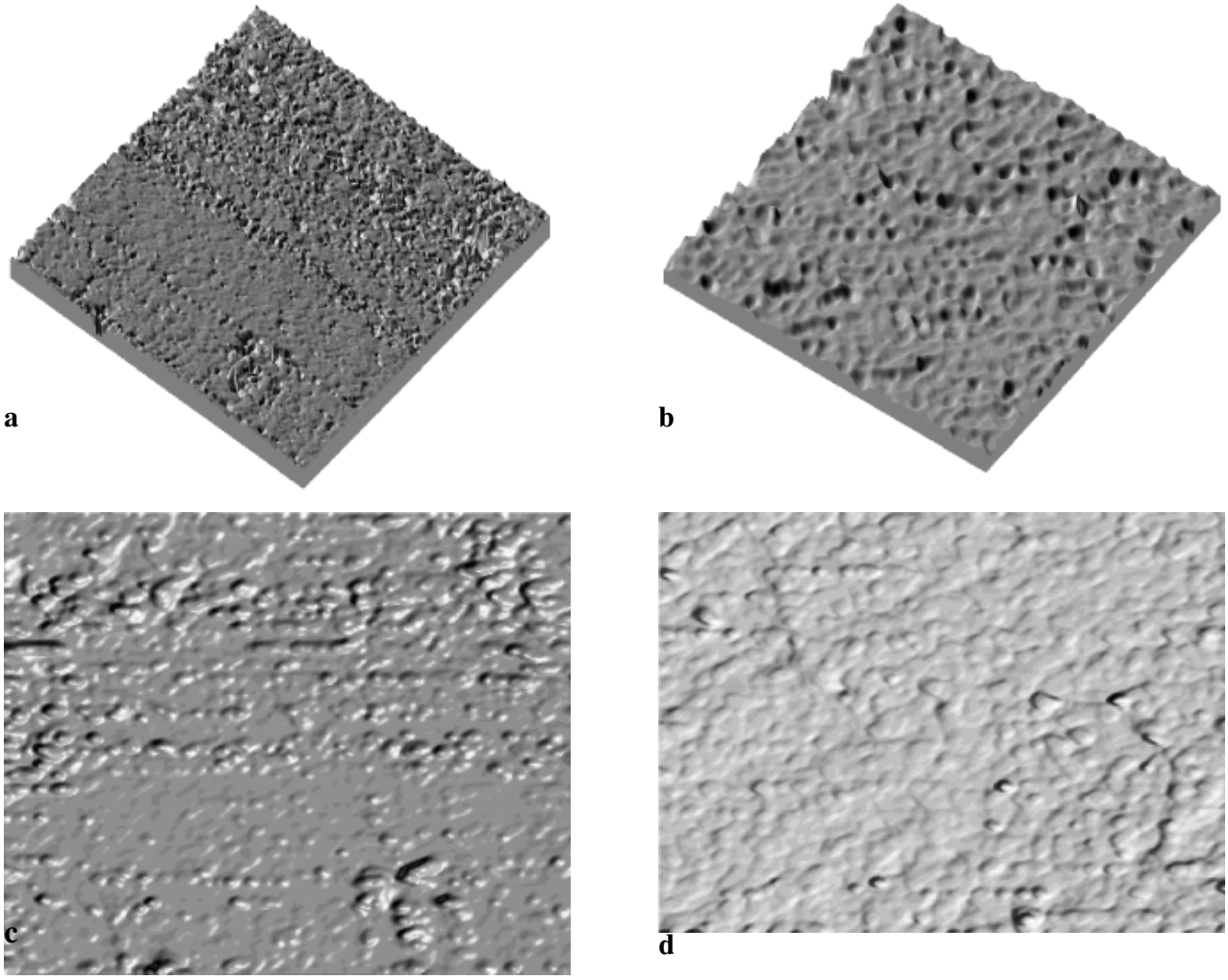

Fig. 7. The STM-images of gold surfaces: polished initial (a, c) and irradiated (b, d) with 253 MeV ^{86}Kr ions up to the fluence 10^{14} ions/cm^2. The areas of scanning and the heights of relief have the values: a – 600 nm × 600 nm × 30.87 nm; b – 556 nm × 556 nm × 8.66 nm; c – 600 nm × 600 nm × 25.79 nm; d – 1200 nm × 1200 nm × 7.54 nm.

Fig. 7d) surface structures of gold samples obtained with the help of STM are presented in Fig. 7. As one can see, the mean relief heights in images (Fig. 7a) and (Fig. 7b) are $H_a \cong 27$ nm and $H_b \cong 12$ nm, respectively [4]. The approximate number of atoms evaporated (sputtered) from the gold surface under ^{86}Kr ion irradiation has been estimated as $N_{AuS} \sim (H_a - H_b) \times N_{Au} = 9.2 \times 10^{16}$ atoms/cm^2, where: $N_{Au} = 5.90 \times 10^{22}$ atoms/cm^3 is the gold atom number density. Thus, the sputtering coefficient (or, most probably, the evaporation coefficient) has an approximate value of $S_{ex} \cong N_{AuS}/(F \cdot t) = 9.2 \times 10^2$ atoms/ion. Comparison between the sputtering/evaporating coefficients for annealed and cold-deformed gold samples irradiated with Kr ions shows that they differ by a factor of ≈900 [4].

Such a high value of the evaporating coefficient in the case of cold-deformed gold can be explained by the processes of gold atom evaporation from the surface under the Kr ion passing through surface only. It means that the temperature in the volume around the projected range of the swift heavy ion in cold-deformed gold samples was higher than the melting point and the evaporation temperature. So the thermal spike model must be used in this case. The approximate temperature in the volume around the ion track may be calculated using the equation (7) [14, 18]:

$$T_{tr}(r,t) = \frac{S_{inel}}{4\pi\chi_L t} \cdot \exp\left(-\frac{C_i r^2}{4\chi_L t}\right) + T_0 \qquad (7)$$

where T_0 is the irradiation temperature (room temperature). To calculate the temperature, we used the following parameter values: heat conductivity $\chi_L = 270$ W/(m·K) at temperature $T = 1000$ K and heat capacity $C_i = 159$ kJ/(kg·K) at temperature $T = 1500$ K. So, we took into account the parameter value for a high temperature. Using expression (5) and the mean value for the crater diameter on the surface of cold-deformed gold samples irradiated with ^{86}Kr ions (Fig. 7b) $D_{ex} \approx 100$–200 Å, one can obtain the temperature at the volume around the ion trajectory, ion track temperature $T_{tr} \approx 4120$–5580 K for the crater diameters values $D_{tr} = 120$–100 Å, respectively. This value of T_{tr} is comparable with the track temperature calculated using expression (2). The melting point and evaporation temperature for gold are much less, i.e. 1336 K and 3150 K, respectively.

In Fig. 8, the temperature T_{tr} as a function of the distance from the beam trajectory axis is presented for different times: $t_1 = 1 \times 10^{-13}$ s (*1*); $t_2 = 2 \times 10^{-13}$ s (*2*) and $t_3 = 3 \times 10^{-13}$ s (*3*). The curves *1–3* were obtained using expression (7) [14, 18].

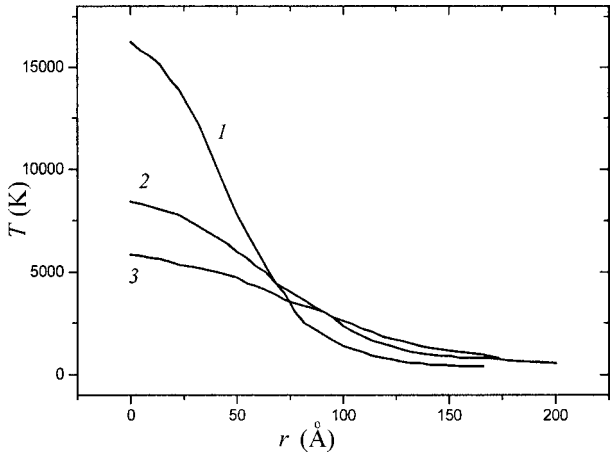

Fig. 8. The temperature as a function of the distance from ion beam trajectory axis for various time: $t_1 = 1 \times 10^{-13}$, $t_2 = 2 \times 10^{-13}$, $t_3 = 3 \times 10^{-13}$ s. See expression (7).

As one can see, the temperatures at the area around the track axis with the radius about 50–75 Å during the time up to 10^{-12} s are higher than the melting point and evaporation temperature for gold.

One can conclude that the sputtering/evaporation coefficient strongly depends on the defect concentration (point defects, defect clusters and drawing defects-dislocations). That conclusion is in agreement with the results obtained for irradiated metals, alloys and HOPG [5, 9, 10].

Conclusion

The presence of radiation defects in metals essentially increases the influence of inelastic energy losses of fast heavy ions on the sputtering yield. Thus, the sputtering yield for a metal having a small number of defects in its crystalline structure is in the range 1–10 atoms/ion [1, 6, 15]. Experiments show that the sputtering yield for coarse-grained metals under swift heavy ion irradiation at high irradiation fluences ($\sim 2 \times 10^{15}$ ions/cm^2) increases significantly (by up to 3 times of orders of magnitude) because of accumulating radiation defects in the target crystalline structure. The experimentally observed high sputtering yield for nickel and gold can be explained by atom evaporation from the track surface which has been heated up to the boiling temperature T_b, i.e. a thermal spike model should be used at high concentrations of damage and initial defects. In this way, we experimentally prove that inelastic energy losses $(dE/dx)_{inel}$ of fast heavy ion have a strong influence on sputtering of the metal with a damaged crystal structure.

The importance of sputtering problem for accelerator engineering and for the high-energy heavy ion implantation into special materials should be a justification for further experimental and theoretical research on swift heavy ion irradiation in the inelastic energy loss region.

References

1. Akapiev GI, Balabaev AN, Vasiliev NA *et al.* (1998) Gold sputtering by krypton ions in inelastic energy loss range. J Tech Phys (Rus) 68;1:134–135
2. Chanel M, Hansen J, Laurent J-M, Madsen N, Mahner E (2001) Experimental investigations of impact-induced molecular desorption by 4.2 MeV/u Pb ions. In: Lucas P, Webber S (eds) Proc of the 2001 Particle Accelerator Conf (PAC 2001), June 18–22, 2001, Chicago, USA. Vol. 3, pp 2165–2167
3. Cheblukov YuN (1999) Coarse-grained structure metal sputtering by swift heavy ions in the inelastic energy loss range. In: Abov YuG, Suvorov AL, Firsov V (eds) Proc of the 1st Int School of Physics Actual Problems of the Nuclear Physics, Condensed Matter Physics and Chemistry, February 17–26, 1998, Zvenigorod, Russia, pp 181–184 (in Russian)
4. Cheblukov YuN, Didyk AYu, Khalil A *et al.* (2001) Sputtering of metals by swift heavy ions with high fluence. In: Abov YuG, Suvorov AL, Firsov VG (eds) Proc of the 15th Int Conf on Ion-Surface Interactions (ISI-2001), August 27–31, 2001, Zvenigorod, Russia. Vol. 1, pp 171–174
5. Cheblukov YuN, Didyk AYu, Khalil A *et al.* (2002) Sputtering of metals by heavy ions in the inelastic energy loss range. Vacuum 166:133–136
6. Cheblukov YuN, Koshkarev DG, Peuto AR, Rudskoygh IV, Vasiliev NA (1992) Sputtering of gold by uranium ions with UNILAC energies. Part Accel 37/38:351–353
7. Davydov AA, Kalinichenko AI (1985) Mechanical effects near ion tracks and thermal peaks. Voprosy Atomnoj Nauki i Tekhniki (Radiation Damage Physics and Radiation Technology) 3;36:27–30
8. Didyk AYu (1995) Heavy ion irradiation effect on chromium-nickel steel at high temperatures. Metally (Rus) 3:128–135
9. Didyk AYu, Semina VK, Khalil A *et al.* (2000) High-energy heavy ion irradiation effect on nickel sputtering. Lett J Tech Phys (Rus) 26;2:1–7
10. Didyk AYu, Semina VK, Stepanov AE, Suvorov AL, Cheblukov YuN, Khalil A (2001) The surface structure changes of Ni, W and stainless steel irradiated with high energy krypton ions. Adv Mater 1:58–64
11. Didyk AYu, Varichenko VS (1995) Track structure in dielectric and semiconductor single crystals irradiated by heavy ions with high level of inelastic energy loss. Radiat Meas 25:119–124
12. Komarov FF, Novikov AP, Burenkov AF (1994) Ion implantation. Minsk University, Minsk (in Russian)
13. Koshkarev DG (1984) The charge-exchange instability in intense ion beams. Part Accel 16:1–4
14. Kulikov DV, Suvorov AL, Suric PA, Trushin YuV, Kharlamov VS (1993) Physical model of formation periodical structure on the surface of pyrolytic graphite at high energy ion irradiation. Lett J Tech Phys (Rus) 23;14:89–93
15. Mieskes HD, Assmann W, Brodale M *et al.* (1998) Measuring sputtering yields of high energy ions on metals. Nucl Instrum Meth Phys Res B 146:162–171
16. Oganessian YuTs, Dmitriev SN, Didyk AYu, Gulbekian GG, Kutner VB (2000) New possibilities of the FLNR accelerator complex for the production of track membranes. In: Proc of the 10th Int Conf Radiation Physics of Solids, 3–8 July, 2000, Sevastopol, Ukraine, pp 42–50
17. Skuratov VA, Illes A, Illes Z *et al.* (1999) Beam diagnostics and data acquisition system for ion beam transport line used in applied research. JINR Communications E13-99-161. JINR, Dubna
18. Yavlinskii Yu (1998) Track formation in amorphous metals under swift heavy ion bombardment. Nucl Instrum Meth Phys Res B 146:142–149